Hydrothermal Synthesis of Monodispersed Octahedral Gold Nanocrystals with Five Different Size Ranges and Their Self-Assembled Structures

Chia-Chien Chang, Hsin-Lun Wu, Chun-Hong Kuo, and Michael H. Huang*

Department of Chemistry, National Tsing Hua University, Hsinchu 30013, Taiwan

Received August 12, 2008. Revised Manuscript Received October 23, 2008

Here we report the hydrothermal synthesis of octahedral gold nanocrystals from an aqueous solution of $HAuCl_4$, trisodium citrate, and cetyltrimethylammonium bromide (CTAB) surfactant. By heating the mixture at 110 °C for 6, 12, 24, 48, and 72 h, gold octahedra with approximate average sizes of 30, 60, 90, 120, and 150 nm can be obtained. The percent yield of octahedral nanocrystals is more than 90% for all the samples. Products formed at shorter reaction times were also examined. Structural characterization confirmed that the octahedra are bounded by entirely {111} faces. As particle size increases, the surface plasmon resonance (SPR) absorption band red-shifts from 543 to 635 nm. These monodisperse gold octahedra can spontaneously self-assemble into long-range ordered packing structures upon water evaporation. Three types of self-assembled structures with faces, edges, or corners of the octahedra contacting the substrates have been identified. Particle size can affect the type of packing structure they adopt. The detailed packing arrangements are described. Significant red-shifted SPR coupling absorption bands in the near-infrared region are observed as a result of the formation of these assembled structures. These gold octahedra have been shown to serve as effective surface-enhanced Raman scattering substrates using thiophenol as the test molecule.

Introduction

Gold nanocrystals with simple geometric shapes such as cubic and octahedral structures have begun to emerge in the past few years.[1−3] The ability to prepare these gold nanocrystals with a high degree of shape control should facilitate the examination of their facet-specific properties. In the few reports available on the synthesis of nanocrystalline gold octahedra, polymers such as polyvinyl pyrrolidone (PVP) and polystyrene-*block*-poly(2-vinylpyridine) (PS-*b*-P2VP) have been used as the capping and shape controlling agents.[4−8] Polyethylene glycol, *n*-pentanol, pentanediol, and toluene have been used in these studies as the solvents. For these methods a more elaborate cleaning procedure may be needed to fully remove the polymers, and there is also a concern of the direct use of these nanocrystals in biological systems. Thus, the development of a synthetic method for octahedral gold nanocrystals in aqueous solution is highly desirable. Other aspects of the octahedral gold nanocrystal growth worth considering include their fine size control over a wide range and the possibility of observing their long-range ordered self-assembled structures. Although particle size control over ranges of 30−60 nm and 33−120 nm in edge length have been reported, it remains a challenge to maintain a good size distribution as particle size increases.[4,5] Submicron-sized gold octahedra show an even larger distribution of sizes.[9] Uniform octahedral nanocrystal building blocks with eight equilateral triangular faces can exhibit extended packing structures on substrates, but fabrication of such superstructures have rarely been demonstrated. Formation of super crystal structures of octahedral *c*-In_2O_3 nanocrystals with different kinds of three-dimensional (3D) self-assembly have been reported recently.[10] Assembly of octahedral silver nanocrystals into macroscopic two-dimensional (2D) superlattices using the Langmuir−Blodgett technique has been achieved.[11] However, no study has shown the 3D self-assembled structures formed by octahedral gold nanocrystals.

Here, we present a simple hydrothermal synthesis approach for the high-yield growth of monodispersed octahedral gold nanocrystals with five size ranges from around 30−150 nm in diameter. Here, the particle diameter refers to the distance from one corner to the opposite corner, or 1.73 times the edge length. CTAB surfactant was used to control the particle morphology. These nanocrystals can spontaneously self-

* To whom correspondence should be addressed. E-mail: hyhuang@mx.nthu.edu.tw.

(1) Seo, D.; Park, J. C.; Song, H. *J. Am. Chem. Soc.* **2006**, *128*, 14863.
(2) Kim, F.; Connor, S.; Song, H.; Kuykendall, T.; Yang, P. *Angew. Chem., Int. Ed.* **2004**, *43*, 3673.
(3) Sau, T. K.; Murphy, C. J. *J. Am. Chem. Soc.* **2004**, *126*, 8648.
(4) Li, C.; Shuford, K. L.; Park, Q.-H.; Cai, W.; Li, Y.; Lee, E. J.; Cho, S. O. *Angew. Chem., Int. Ed.* **2007**, *46*, 3264.
(5) Zhang, J.; Liu, H.; Wang, Z.; Ming, N. *Appl. Phys. Lett.* **2007**, *90*, 163122.
(6) Yamamoto, M.; Kashiwagi, Y.; Sakata, T.; Mori, H.; Nakamoto, M. *Chem. Lett.* **2007**, *36*, 1348.
(7) Seo, D.; Yoo, C. I.; Park, J. C.; Park, S. M.; Ryu, S.; Song, H. *Angew. Chem., Int. Ed.* **2008**, *47*, 763.
(8) Zhang, J.; Gao, Y.; Alvarez-Puebla, R. A.; Buriak, J. M.; Fenniri, H. *Adv. Mater.* **2006**, *18*, 3233.
(9) Liu, X.; Wu, N.; Wunsch, B. H. Jr.; Stellacci, F. *Small* **2006**, *2*, 1046.
(10) Lu, W.; Liu, Q.; Sun, Z.; He, J.; Ezeolu, C.; Fang, J. *J. Am. Chem. Soc.* **2008**, *130*, 6983.
(11) Tao, A.; Sinsermsuksakul, P.; Yang, P. *Nat. Nanotechnol.* **2007**, *2*, 435.

10.1021/cm8021984 CCC: $40.75
Published on Web 11/24/2008

assemble into regions of 3D packing structures with different orientations on the substrates upon evaporation of water. Solution and solid phase UV−vis absorption spectra of the isolated and assembled nanocrystals were taken to reveal significant spectral shifts. These octahedral nanocrystals can serve as effective surface-enhanced Raman spectroscopy (SERS) substrates and such application was also examined.

Experimental Section

Hydrogen tetrachloroaurate trihydrate ($HAuCl_4 \cdot 3H_2O$, Aldrich, 99.9%), cetyltrimethylammonium bromide (CTAB, Aldrich, 95%), and trisodium citrate ($Na_3C_6H_5O_7 \cdot 2H_2O$, Mallinckrodt, 99.9%) were used without further purification. For the hydrothermal synthesis of octahedral gold nanocrystals, 9.7 mL of ultrahigh purity water, 0.055 g of CTAB, 250 μL of 0.01 M $HAuCl_4$, and 50 μL of 0.1 M trisodium citrate were added to a glass vial with a Teflon-lined polypropylene cap and a volume capacity of 22.5 mL. CTAB concentration in the final solution is 1.51×10^{-2} M. The oven temperature was set at 110 °C. Sample vials were loaded into the oven after it had reached this temperature. Sample vials A−E wrapped in aluminum foil were respectively heated for 6, 12, 24, 48, and 72 h. After that, the vials were removed from the oven and cooled naturally to room temperature. UV−vis absorption spectra of these solutions were taken. To remove the residual CTAB surfactant, the solutions were centrifuged at 6000 rpm for 20 min (Hermle Z323 centrifuge). The supernatant was decanted, and the precipitate was redispersed in deionized water for another round of centrifugation. Finally the nanocrystals were stored in deionized water. Scanning electron microscopy (SEM) characterization of the nanocrystals was performed by using a JEOL JSM-7000F scanning electron microscope. A drop of the concentrated nanocrystal solution was added onto a silicon substrate and dried under ambient condition. Normally it takes about 2 h to completely evaporate water. Transmission electron microscopy (TEM) characterization was carried out by using a JEOL JEM-2100 transmission electron microscope operating at 200 kV. X-ray diffraction (XRD) patterns were collected with the use of a Shimadzu XRD-6000 diffractometer with Cu Kα radiation. UV−vis absorption spectra were taken on a JASCO V-570 spectrophotometer. To obtain absorption spectra of the self-assembled structures of the octahedral gold nanocrystals, a drop of the concentrated nanocrystal solution was added to the inside wall of a flat-lying quartz cuvette in the light path of the measuring spectrophotometer and dried in the air. For the Raman and SERS spectra, 1.0×10^{-4} M thiophenol (AVOCADO, 97%), diluted from an ethanol solution with a concentration of 1.0×10^{-2} M, in the aqueous Au octahedra solution with particle sizes of ~30, 60, and 90 nm from samples A, B and C were prepared. Samples were excited with a He−Ne laser at 632.8 nm (Melles-Griot, 15 mW). The scattered light was collected with a Princeton Instrument system equipped with a thermoelectric cooled CCD detector.

Results and Discussion

The products formed were mainly examined by scanning electron microscopy. Figure 1 shows the SEM images of the five samples made with different reaction times. As can be seen, all of the samples contain mostly octahedral nanocrystals, and the particles form extended self-assembled structures on the substrates. The nanocrystals also appear to be highly monodisperse in size, facilitating their spontaneous organization into well-ordered packing structures. Table 1 gives the average particle sizes, their standard deviations,

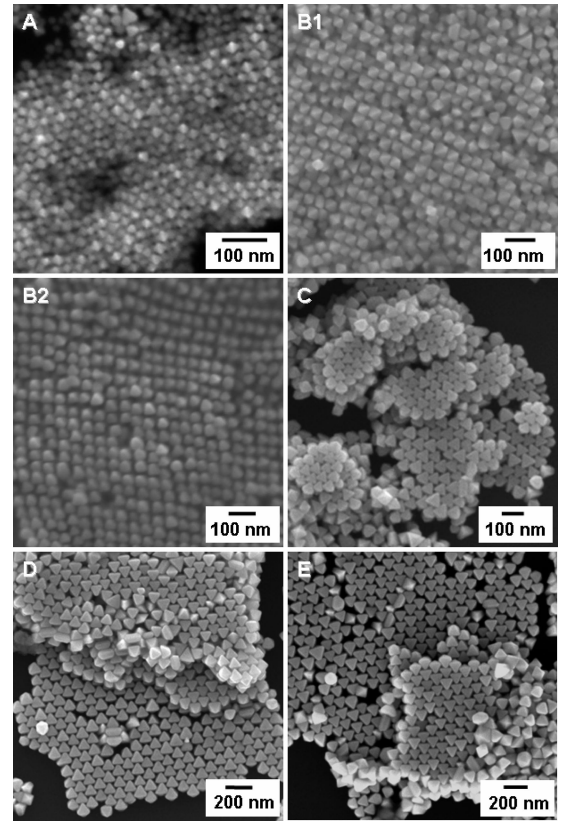

Figure 1. SEM images of the octahedral gold nanocrystals for samples A-E with average diameters of 31, 57, 89, 119, and 149 nm. The imaged regions show extensive self-assembled structures. Two types of packing order are shown for sample B.

Table 1. Average Particle Sizes, Standard Deviations, and Percent Yields of the Octahedral Gold Nanocrystals in Samples A−E

sample	particle size (nm)	standard deviation (%)	percent yield (%)
A (6 h)	31 ± 3	10.9	96
B (12 h)	57 ± 4	7.3	96
C (24 h)	89 ± 8	8.6	94
D (48 h)	119 ± 8	6.7	92
E (72 h)	149 ± 9	6.0	91

and the percent yields of the five samples. Octahedral gold nanocrystals in samples A−E have average particle diameters of 31, 57, 89, 119, and 149 nm (see the Supporting Information for the size distribution histograms). Particle size increases with a longer reaction time. With the exception of sample A, all the other samples have standard deviations of the particle sizes below 10%. Significantly, over 90% of the products obtained are octahedral gold nanocrystals. The byproducts are mainly thick triangular nanoplates of similar sizes to the octahedra with possibly {111} side facets. They may be considered as highly truncated trigonal bipyramids. The thick nanoplates can stack face-to-face and form a packing order with the assistance of the underlying octahedra or nanoplates (see the Supporting Information). From Figure 1, one can see that samples A and B exhibit one type of self-assembled structure with the plane formed by the top and bottom edges of the octahedra being perpendicular to the substrate surface (i.e., panels A and B1). Octahedra in sample B also display another type of packing structure with their corners pointing up (i.e., panel B2). A more common self-assembled pattern is observed for samples C−E, in

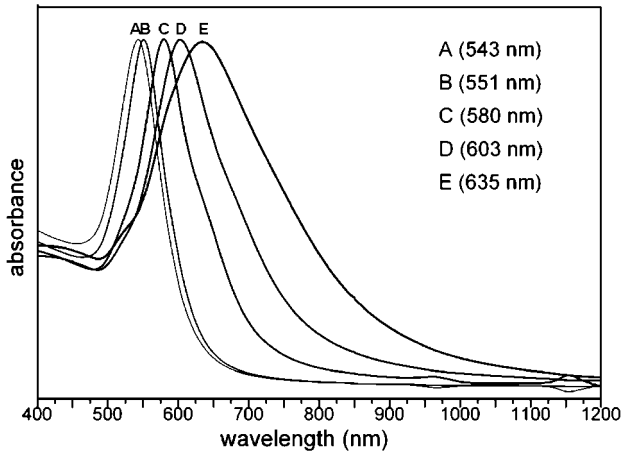

Figure 2. UV−vis absorption spectra of samples A−E. Maximum absorbance of the spectra has been normalized.

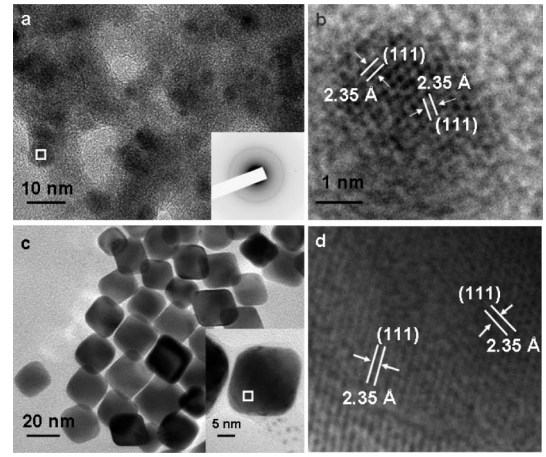

Figure 3. (a) TEM image of the ultrasmall gold nanoparticles produced after 1 h of reaction. The inset shows the corresponding SAED pattern, which can be indexed to the face-centered cubic structure of gold. (b) High-resolution TEM image of a single gold nanoparticle found in the square region of panel a. (111) lattice planes can be observed with a measured *d*-spacing of 2.35 Å. (c) TEM image of the octahedral gold nanocrystals synthesized after 3 h of reaction. The inset shows a single gold octahedron. (d) High-resolution TEM image of the square region in the inset of panel c. Lattice fringes with a *d*-spacing of 2.35 Å corresponding to the Au (111) planes was measured for both sets of lattice planes.

which the octahedral gold nanocrystals sit on their triangular faces. This packing structure is also observable for sample B. The detailed analysis of these superstructures will be presented later.

Figure 2 shows the UV−vis absorption spectra of the samples A-E, revealing slight color changes of the nanoparticle solutions. Photographs of the five samples are provided in the Supporting Information. As particle size of the octahedral gold nanocrystals increases, the surface plasmon resonance (SPR) absorption band red-shifts from 543 nm for sample A to 635 nm for sample E. The absorption band also gets wider for particularly samples D and E due to a broader range of their particle sizes and possibly the excitation of two in-plane dipole modes.[4] The presence of a shoulder band to the long-wavelength side of the main SPR band should be related to the anisotropic shape of an octahedron.[4] The thick triangular nanoplate byproducts may also contribute to this shoulder band.

The crystal structure of these octahedral gold nanocrystals has been characterized by XRD and TEM techniques (see the Supporting Information). XRD pattern of the products synthesized in sample E reveals that the intensity of the (111) reflection peak is extremely strong compared to those of the (200) and (220) peaks. The result indicates that the octahedra are bounded by entirely {111} faces, and that they deposit preferentially with their triangular faces on the substrate surface. It also supports the view that the triangular nanoplate byproducts are also bounded by the {111} facets. Selected-area electron diffraction (SAED) analysis of a single octahedral gold nanocrystal gives a diffraction pattern which is consistent with the face-centered cubic structure of gold. Although TEM images of small areas of the gold octahedra with close-packed monolayer structure can be obtained, larger regions of such assembled structures cannot be found, possibly because of the tendency of breaking the carbon support film on the copper grid under the weight of such extended nanocrystal packing structures.

Because the reaction times used here are quite long compared to those used to make triangular and hexagonal gold nanoplates by a thermal aqueous solution approach, we have also examined the products formed after shorter reaction times (see Figure 3).[12,13] Ultrasmall particles of roughly octahedral shape with sizes of less than 5 nm were observed after 1 h of reaction. Sets of lattice planes with a *d*-spacing of 2.35 Å were measured, which should correspond to the Au (111) lattice planes. After 3 h of reaction, octahedral gold nanocrystals were synthesized. They have diameters of approximately 25−30 nm, but the product yield is low from the TEM and UV−vis absorption characterization. Thus, the octahedral crystal morphology is established when the particles are just a few nm in size, but the growth rate is considerably slow. We speculate that the reason the nanocrystal growth is so slow because oxygen present in this closed system may act as an oxidizing agent ($O_2 + 4H^+ + 4e^- \rightarrow 2H_2O$) and slowly dissolve the gold atoms into the solution ($Au + 4Cl^- \rightarrow AuCl_4^- + 3e^-$). This side reaction makes gold nanocrystal growth be extremely slow. Because of the slow reaction rate under the present hydrothermal synthesis conditions and in the absence of other structure-modifying ions, octahedra and thick triangular nanoplates with entirely {111} faces are considered to be the thermodynamically favorable product structures. In addition, the use of trisodium citrate to enhance the formation of the (111) planes has been suggested.[12] Another important factor governing the preferential growth of octahedral nanocrystals is the molar ratio of [CTAB]/[$HAuCl_4$]. A [CTAB/$HAuCl_4$] molar ratio of 60 was used in this study for the synthesis of octahedral gold nanocrystals in high yield. When the molar ratio is 7.5 and the reaction time is 24 h, nanoplates with sizes of hundreds of nanometers and decahedra and icosahedra with diameters of ~250 nm were collected (data not shown). Previously, a [CTAB/$HAuCl_4$] molar ratio of 6 was used for the preparation of gold nanoplates by a thermal aqueous solution approach.[12] At a molar ratio of 15,

(12) Chu, H.-C.; Kuo, C.-H.; Huang, M. H. *Inorg. Chem.* **2006**, *45*, 808.
(13) Huang, W.-L.; Chen, C.-H.; Huang, M. H. *J. Phys. Chem. C* **2007**, *111*, 2533.

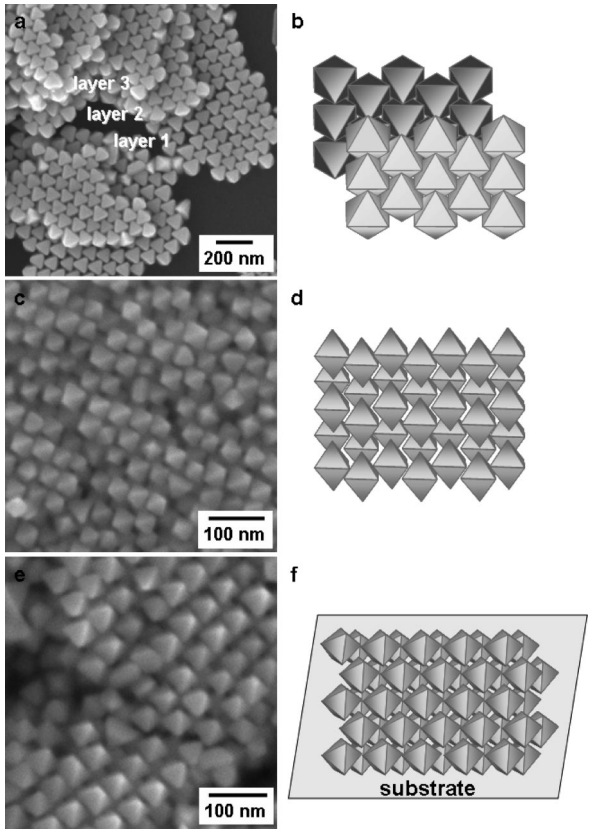

Figure 4. SEM images of the three types of self-assembled structures of the octahedral gold nanocrystals with particle sizes of (a) 120 and (c, e) 60 nm. (b, d, f) Schematic drawings of the three types of nanocrystal packing order. Drawing f resembles the viewing direction of panel e with the underlying substrate.

octahedra with diameters of ~150−200 nm were produced along with the formation of a significant fraction of triangular nanoplates. Use of a molar ratio of 100 resulted in the growth of more uniformly sized octahedra of ~35 nm in diameter and few nanoplates. The critical micelle concentration (cmc) value for CTAB at 60 °C is 1.0 mM.[14] The concentration of CTAB used here for the synthesis of gold octahedra is significantly higher than the cmc (i.e., 15.1 mM). This condition appears to be critical for the high-yield and size-controlled growth of octahedral gold nanocrystals.

Representative SEM images of the three types of self-assembled structures of the octahedral gold nanocrystals and their schematic illustrations are shown in Figure 4. SEM images of the three types of packing structures over large areas are given in the Supporting Information. For the type I self-assembled structure, octahedra contact each other by their faces to form a close-packed monolayer (panels a and b in Figure 4). The second layer has the same packing arrangement as the first layer. We observed that the upper layer has a great tendency to deposit on the bottom layer via complete or partial face-to-face contact, possibly because this deposition condition can minimize the free energy for such layer-by-layer assembly. This leads to opposite and alternate packing orientations for the adjacent layers of gold octahedra. Thus, octahedra in layer 1 has the same packing direction as octahedra in layer 3, but different from octahedra in layer 2. Because of the lack of strong forces or interactions between the layers, formation of just 2−3 layers is typically observed. This type of self-assembled structure is observed for octahedra with sizes of 90−150 nm, presumably because the larger gold octahedra deposit faster on the substrate with their triangular faces to enhance this single-layer assembly. Type II self-assembled structure is distinctly different from that of type I structure (parts c and d in Figure 4). Here the octahedra form 3D multilayer face-touching superstructure with their edges contacting the underlying substrate. This is also a stable packing arrangement, but requires the formation of a more extensive array of these interlocking octahedra to establish the strength necessary for deposition on their edges. To form type II self-assembled structure, we suspect the octahedra should spend more time in the droplet before evaporation to build such a long-range ordered structure. Thus, only smaller and lighter octahedral gold nanocrystals with sizes of 30−60 nm were observed to form type II structure. Type III self-assembled structure is closely related to type II structure, but with their corners contacting the substrate surface (parts e and f in Figure 4). The 3D packing arrangement is the same as that observed for type II structure, but as the array is formed in the solution the octahedra have their corners pointing toward the substrate. Type III structure results as they settle on the substrate. Figure 4d can be used to see the side view of this packing structure if a line is drawn below the bottom three octahedra to symbolize the substrate. Again this seemingly unstable structure can only exist as large arrays for stability reason, and only octahedra with sizes of ~60 nm from sample B exhibit type III superstructure. Surprisingly, none of these assembled structures matches any of the packing patterns observed for c-In_2O_3 nanocrystals, where either edge-sharing and/or corner-touching arrangements were obtained.[10] Differences in the particle sizes, capping agents, and solvents used and the drying process should strongly affect the assembly of octahedral nanocrystals. The three types of packing structures are reproducible by the simple water evaporation approach adopted. Temperature and pressure used for the evaporation of water (i.e., room temperature and atmospheric pressure) are the same for all the samples, and in all the cases concentrated octahedral nanocrystal solutions were dropped onto the substrates. Finer control of these parameters and possible surface functionalization to form more extended areas of packing structures will be explored.

The octahedral gold nanocrystals with extensive self-assembled structures in the solid phase should display uniquely different absorption features. Figure 5 presents the UV−vis absorption spectra of the octahedral nanocrystals on the side wall of a quartz cuvette for samples B−D. In addition to the absorption bands expected for the more isolated octahedra, a broadband extending to the near-infrared region is recorded for each sample with approximate band maxima at 750, 1130, and 1300 nm for octahedra in samples B−D, respectively. This band is attributed to the coupling of SPR absorption from the formation of octahedra superstructures, as have been observed in other assembled gold

(14) Myers, D.; *Surfactant Science and Technology*; VCH: New York, 1988; pp 118−119.

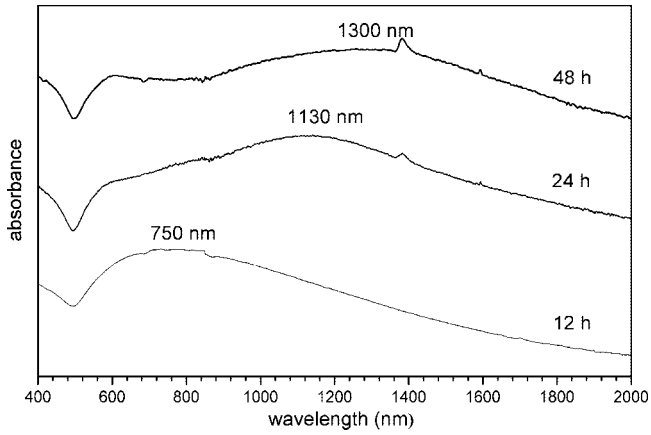

Figure 5. UV−vis absorption spectra of the octahedral gold nanocrystals in the solid phase for samples B−D.

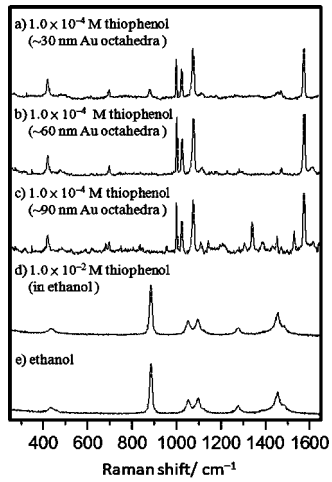

Figure 6. (a−c) SERS spectra of 1.0×10^{-4} M thiophenol in the gold octahedra solution with particle sizes of ∼30, 60, and 90 nm from samples A, B, and C. A 1.0×10^{-2} M thiophenol solution in ethanol was prepared first and diluted with the Au octahedra solution to make its final concentration be 1.0×10^{-4} M. The excitation wavelength is 632.8 nm. (d) Raman spectrum of 1.0×10^{-2} M thiophenol in ethanol. In the absence of the gold octahedra, only Raman spectrum of ethanol was obtained despite a higher concentration of thiophenol in the solution. (e) Raman spectrum of ethanol.

nanostructures.[15−17] The strong plasmon coupling leads to the observation of these substantially red-shifted SPR absorption bands. The larger gold octahedra may form better particle-to-particle contacts over greater areas that their plasmon coupling bands appear at longer wavelengths.

The use of these gold octahedra as SERS substrates was also examined. Previously SERS properties of 2-naphthalenethiol (2-NAT) on polymer films of gold octahedra have been studied.[8] The octahedral gold nanocrystals with sizes of ∼30, 60, and 90 nm from samples A−C were used as SERS substrates for thiophenol (see Figure 6). In the absence of the gold octahedra, Raman signals of thiophenol were not measured despite its high concentration of 1.0×10^{-2} M in ethanol. Dilution of thiophenol to 1.0×10^{-4} M in the gold octahedra solution resulted in the collection of strongly surface-enhanced Raman scattering signals for all three samples, confirming that these octahedral gold nanocrystals can serve as effective SERS substrates. The SERS spectra of thiophenol obtained are consistent with the reported spectra.[18−20] Characteristic C−C stretching bands of surface thiophenol at 999, 1022, and 1075 cm^{-1} were recorded. The 1075 cm^{-1} band can also be assigned to the C−S stretching and C−H bending modes.[18] Gold octahedra with an average particle size of 90 nm exhibit a better enhancement property than those of the 30 and 60 nm octahedral particles. This effect presumably is related to the presence of a larger local electromagnetic field caused by the more efficient SRP absorption of the 90 nm gold octahedra at the exciting wavelength of 632.8 nm used.[20] Surprisingly, no SERS signals were measured for gold octahedra with sizes of ∼120 nm. This result suggests that gold octahedra with sizes greater than 100 nm are not suitable for use as SERS substrates. Similar observations have been made with the use of icosahedral gold nanoparticles as SERS substrates.[21] Strong SERS peaks were recorded for icosahedral gold nanoparticles with sizes of ∼32 nm, but drastic loss of SERS signals occurred as particle sizes increased to ∼70 nm.

Conclusion

In conclusion, we have successfully synthesized monodisperse octahedral gold nanocrystals with approximate sizes of 30, 60, 90, 120, and 150 nm by the hydrothermal synthesis approach. The percent yields of octahedral particles in the samples are over 90%. Their structure has been examined by XRD, SEM, and TEM techniques. These monodisperse gold octahedra can spontaneously self-assemble into long-range-ordered packing structures upon water evaporation. Three types of assembled patterns on the substrates have been identified. The formation of such assembled structures allows the observation of significant red-shifted SPR coupling absorption bands in the near-infrared region. The use of these octahedral gold nanocrystals as effective SERS substrates was also demonstrated. It is expected that these size-controlled gold octahedra synthesized in aqueous solution and their assembly should find more applications such as in molecular sensing and tunable plasmonic response.

Acknowledgment. We thank Jung-Wei Ling and Prof. I-Chia Chen for assistance in the collection of Raman spectra. Financial support for this work is provided by the National Science Council of Taiwan (Grant NSC95-2113-M-007-031-MY3).

Supporting Information Available: Size distribution histograms, SEM image of the thick triangular nanoplate side product, photographs of the five sample solutions, XRD pattern and TEM images of the octahedral gold nanocrystals, and SEM images of the large-area packing structures (PDF). This material is available free of charge via the Internet at http://pubs.acs.org.

CM8021984

(15) Thomas, K. G.; Barazzouk, S.; Ipe, B. I.; Joseph, S. T. S.; Kamat, P. V. *J. Phys. Chem. B* **2004**, *108*, 13066.
(16) Chen, C.-F.; Tzeng, S.-D.; Chen, H.-Y.; Lin, K.-J.; Gwo, S. *J. Am. Chem. Soc.* **2008**, *130*, 824.
(17) Ghosh, S. K.; Pal, T. *Chem. Rev.* **2007**, *107*, 4797.
(18) Tayor, C. E.; Pemberton, J. E.; Goodman, G. G.; Schoenfisch, M. H. *Appl. Spectrosc.* **1999**, *53*, 1212.
(19) Bhuvana, T.; Pavan Kumar, G. V.; Kulkarni, G. U.; Narayana, C. *J. Phys. Chem. C* **2007**, *111*, 6700.
(20) Kim, K.; Lee, H. B.; Lee, J. W.; Park, H. K.; Shin, K. S. *Langmuir* **2008**, *24*, 7178.
(21) Kwon, K.; Lee, K. Y.; Lee, Y. W.; Kim, M.; Heo, J.; Ahn, S. J.; Han, S. W. *J. Phys. Chem. C* **2007**, *111*, 1161.